**Programming Energy–Bio Interfaces through Ligand-Directed Electronic Transport in Atomically Precise Gold Nanoclusters**

Soumen K. Dubey[1], Suman Mondal[2], Kajal Gupta[3], Kalyani Iswar[4], Rathindranath Biswas[5], Pritha Chakraborty[6], Aravind Kumar Rengan[4], Suprabhat Mukherjee[6], Pratip Chakraborty[7,8], Kalisadhan Mukherjee[2*], and Rohit K. Sharma[1*]

[1] Department of Chemistry & Centre of Advanced Studies, Panjab University, Chandigarh-160014, India *Email: rohitksg@pu.ac.in

[2] Department of Chemistry, Pandit Deendayal Energy University, Gandhinagar-382426, Gujarat, India

[3] Department of Chemistry, Nistarini College, Purulia-723101, West Bengal, India

[4] Department of Biomedical Engineering, Indian Institute of Technology Hyderabad, Kandi-502284, Telangana, India

[5] Department of Chemistry, Indian Institute of Technology Bombay, Powai-400076, Mumbai, India

[6] Integrative Biochemistry & Immunology Laboratory (IBIL), Department of Animal Science, Kazi Nazrul University, Asansol-713340, West Bengal, India

[7] Cradle Fertility Centre, 496/1, Diamond Park, Joka, Kolkata 700104, West Bengal, India

[8] Assisted Reproduction Technology Division, Institute of Reproductive Medicine, Salt Lake City, Kolkata-700106, West Bengal, India

# Contents

## 1. Instrumentation and Method of Analysis

The $^{1}H$ NMR and $^{13}C$ NMR spectra were measured on a Bruker AVANCE NEO 500 MHz FT NMR Spectrometer. Mass spectra were collected by using Alliance 2795 system coupled to a Q-TOF micro-mass spectrometer, Waters Corporation. The UV-Visible spectra were obtained using Jasco V-750 spectrophotometer at room temperature. HR-TEM and EDS were measured using HRTEM (Model: JEOL; JEM 2100 plus) with Hitachi (H-7500) microscope. The Malvern zeta sizer nano s90 was used to analyze the surface charge and hydrodynamic radius. Fluorolog-3 spectrophotometer was used to record fluorescence spectra. Circular Dichroism (CD) spectra were obtained using Jasco J-1500 spectrometer. FT-IR spectra were obtained in the 400-4000 $cm^{-1}$ range on Perkin Elmer ASCII PEDS 1.60 spectrometer. Powder X-ray diffraction (PXRD) were analyzed using Empyrean, Malvern P-analytical instrument using Cu K-alpha (1.54 Å) radiation. Thermogravimetric analysis (TGA) and DSC-analysis was carried out using (DSCQ20 calorimeter, TA Instruments) in the temperature range of 25-800° C at a heating rate of 20° C/min under nitrogen atmosphere. XPS analysis was conducted using a Thermo Nexsa system with Al Kα source under ultra-high vacuum ($10^{-8}$ mbar), using a 200eV pass energy and 10 ms dwell time, with binding energies recorded from 0–1350 eV. Electrical transport measurements, including DC current–voltage characteristics and magnetoresistance, were carried out using a Keithley 2450 source-measure unit, a Keithley 6221 precision current source, and a Keithley 2182A nanovoltmeter. Frequency dependent experiments were carried out by using LCR meter (Agilent E4980A). Cyclic voltammetry (CV) and amperometry measurements were performed at room temperature using a Metrohm Autolab VIONIC electrochemical workstation (Potentiostat 1, Switzerland) controlled by INTELLO software.

### 4.3.1 NMR Analysis

The $^{1}H$ NMR and $^{13}C$ NMR spectra were measured using DMSO-$d_6$ as the solvent with tetramethyl silane (TMS) as the internal standard at room temperature. The following abbreviations were used to explain the multiplicities: s = singlet, d = doublet, dd = doublet of doublet, t = triplet, q = quartet, m = multiplet. Chemical shifts of NMR spectra were given in parts per million (ppm) with respect to TMS. Chemical shifts of the residual protonated solvent of DMSO-$d_6$ resonance in the $^{1}H$ spectrum at $\delta$ 2.50 ppm and DMSO-$d_6$ resonance

in the $^{13}C$ spectrum at $\delta$ 39.52 ppm have been considered. All coupling constants ($J$ values) were reported in Hertz (Hz).

### 4.3.1 Mass Spectroscopy (MS)

MS were recorded by using Alliance 2795 system coupled to a Q-TOF micro-mass spectrometer, Waters Corporation, U.K. For this analysis, the samples were dissolved in HPLC grade methanol). The obtained spectra were processed using the instrument's proprietary software (Mass Lynx).

### 4.3.2 Native Polyacrylamide Gel Electrophoresis (PAGE)

Native PAGE separation was carried out using a vertical gel electrophoresis unit, and 15:1 acrylamide: bis(acrylamide) ratio. The elution was done using standard TBE buffer (89 mM Tris, 89 mM boric acid, 2 mM ethylenediaminetetraacetic acid) at a cool temperature. The aqueous solution of the sample was then loaded onto the stacking gel (20 µL per well), and eluted for 2 h at a constant voltage mode (150 V) to achieve sufficient separation. The gel was imaged under ultra-violet gel documentation system (Gel Doc XR + System, BioRad, USA).

### 4.3.3 HRTEM, SAED and EDS

The morphology, size distribution, and crystallographic nature of the gold nanoclusters (NDLA-AuNCs) were analyzed using HRTEM. For that purpose, the TEM specimens were prepared by drop-casting a dilute aqueous dispersion of AuNCs on the ultrathin glassy carbon coated copper grids, and the grid was dried under ambient conditions prior to analysis. The average particle size distribution was determined by measuring the diameters of more than 50 individual nanoclusters using ImageJ software, and the result was reported as mean diameter ± standard deviation.

### 4.3.4 FT-IR Analysis

FT-IR spectra were obtained in the 400-4000 $cm^{-1}$ range. For solid state measurements, at first, a background spectrum of the sample holder was recorded under identical conditions and then the samples (5-10 mg) were put on the sample holder, and scanning the spectra in the range of 4000- 400 $cm^{-1}$ with a spectral resolution of 4 $cm^{-1}$, averaging 32 scans per sample to improve the signal-to-noise ratio. A background spectrum of the sample holder was recorded under identical conditions and automatically subtracted.

### 4.3.5 XPS Analysis

XPS analysis were conducted with Al Kα source under ultra-high vacuum ($10^{-8}$ mbar), using a 200eV pass energy and 10 ms dwell time, with binding energies recorded from 0–1350 eV. Prior to analysis, the samples were deposited onto a conductive substrate (such as silicon wafer, indium tin oxide (ITO), or carbon tape) by drop-casting a dispersion of samples, and dried under vacuum to remove the residual solvent. No sputtering was applied to avoid beam-induced reduction. The quantitative analysis of the elemental composition was conducted using sensitivity factors provided by the instrument manufacturer.

### 4.3.6 Spectroscopic Measurements

UV-vis and Fluorescence spectrum were recorded after dissolving the samples in water and then the spectrum was recorded from 200-800 nm for UV-vis and 800-1400 nm with excitation of 690 nm using 800 nm long band pass filter. For CD measurement, the solution of the samples (1 mg. $mL^{-1}$) was measured from 190-600 nm.

For excitonic-coupling analysis, the UV-vis and CD spectra of the AuNCs (1 mg. $mL^{-1}$) were collected and plotted in a staggered fashion using Origin-Pro 8.5 to determine whether a zero-crossing CD signal coincides with the absorption maximum, indicative of excitonic coupling. To quantitatively assess the degree of optical activity, the anisotropy factor g(λ) was calculated across the spectral range using the following equation:

$$g(\lambda) = \theta(\lambda) / (32{,}980 \times A(\lambda))$$

where, θ (λ) is the ellipticity in millidegrees (mdeg) and A (λ) is the corresponding absorption.

### 4.3.7 Electrical Conductivity Measurement

For the conductivity measurements the samples were deposited on an insulating glass substrates using a vacuum-assisted spin-coating technique. Electrical contacts were fabricated in a two-probe configuration. Commercially available silver paint was used to form the electrodes, and copper wires (25–50 μm in diameter) were attached to the sample using silver paste. For DC and magneto-DC measurements, the two contacts were positioned at opposite ends of the sample to ensure uniform current flow along the measurement axis. The prepared samples were then mounted on a suitable sample holder and loaded into a cryostat operating under vacuum for cryogenic studies.

### 4.3.8 Electrochemical and Redox Activity

The redox behaviour of the AuNCs was investigated by cyclic Voltammetry (CV) measurement in a 0.1 (M) TBAF/ acetonitrile electrolyte, using an $Ag/AgNO_3$ reference electrode.

Electrochemical measurements were carried out using a standard three-electrode system consisting of a glassy carbon electrode (GCE, 3 mm diameter) as the working electrode, an Ag/AgCl reference electrode, and a platinum wire as the counter electrode. The GCE was mechanically polished using alumina slurries of decreasing particle size (1 μm, 0.3 μm, and 0.05 μm), followed by rinsing with EtOH and deionized (DI) water to remove surface impurities and ensure a clean, reproducible surface.

To calculate the electrochemical band gap for the AuNCs, following standard equation was used:

$E_{RHE} = E_{Ag/Ag^+} + E + 0.059 \times pH$……..... (1)

Where, $E_{RHE}$ = the corresponding potential for RHE,

$E_{Ag/Ag^+}$ = the standard electrode potential for the $Ag/Ag^+$ couple, and

E= the observed potential using the $Ag/Ag^+$ couple

Using the above equation, the onset oxidation and reduction potentials were found to be -0.16 V and -0.95, respectively.

$E_{ox\ RHE} = 0.799 - 0.16 + 0.413 = 1.052$ V

$E_{red\ RHE} = 0.799 - 0.95 + 0.413 = 0.262$ V,

Herein, the following formula was utilized to determine the experimental electrochemical HOMO and LUMO levels in terms of eV unit:

E (HOMO) = -e [$E_{ox}$ onset + 4.4] …. (2)

E (LUMO) = -e [$E_{red}$ onset + 4.4] …. (3)

And the HOMO and LUMO levels were found to be 4.652 and 4.832 eV respectively having a band gap of 0.8 eV.

E (HOMO) = -e [1.052 - 0.41 + 4.4] = 5.042 eV

E (LUMO) = -e [0.262 - 0.41 + 4.4] = 4.242 eV

### 4.3.9 Fabrication of working electrode

To prepare the working electrode, 3 mg of catalyst was taken in a 1.5 mL micro centrifuge tube and dissolved with a mixed solution of 130 μL of double distilled water (18.2 Milli-Q) and 150 μL of isopropanol. Afterwards, the resulting mixture was sonicated for 30 minutes prior to addition of 20 μL 5% Nafion solution and further sonication was continued using GT-sonic ultra-sonicator for another 15 min to obtain a homogeneous ink. The as-prepared 70 μL catalyst ink was drop-coated onto the Gas Diffusion Layer carbon paper (GDL-CP)

having an area of 0.42 $cm^2$ (6 mm×7 mm) and then it was left for drying in desiccator (under mild vacuum) for overnight. The resulting electrode was used as working electrode (WE) for the study of hydrogen evolution reaction (HER).

For the electrochemical characterizations the samples were coated carbon electrode as working electrode. Graphite rod was used as a counter electrode for HER studies in all electrolyte medium. Whereas Hg/HgO electrode was taken as reference electrode for HER in alkaline medium. The linear sweep voltammetry (LSV) was carried out with a scan rate of 10 mV $s^{-1}$ for HER study. The electrochemical impedance spectroscopy (EIS) was carried out over the frequency range of 100 kHz to 0.1 Hz at an overpotential of 200 mV. All the potentials were converted to RHE using the following Nernst equation for HER activities in alkaline medium:

$$E_{RHE} = E_{working} + 0.059\ pH + E_{Hg/HgO}$$

### 4.3.9 *In Vitro* Cytotoxicity Studies

The colorimetric MTT assay was used to test the viability of normal cells (NIH-3T3 & C2C12 cell lines) as well as triple-negative breast cancer cell line 4T1 with NDLA-AuNCs material. Here, 96-well culture plate was used to seed the 10,000 cells per well and kept for overnight incubation. The cells were treated with NDLA-AuNCs at various doses (0.05-0.4 mg. $mL^{-1}$) in the next day. After 24 h of incubation, MTT (5 mg/mL) in DMEM (without FBS) was replaced with old culture media (DMEM) and kept for incubation for 4 h at 37 °C. The formazan crystals were dissolved using 100 μL of DMSO added to each well, and a multimode plate reader was used to record the absorbance.

$$\%\ \textbf{Cell Viability} = \frac{(\textbf{Absorbance of treated cells})}{(\textbf{Average absorbance of control cells})} \times \mathbf{100}$$

### 4.3.10 Statistical Analysis of *In Vitro* Studies

All the data values were recorded and represented as mean ± standard error of the mean (SEM). Statistical comparisons among multiple groups were performed using one-way analysis of variance (ANOVA), followed by Dunnett's post hoc test by comparing each treatment group with the corresponding control group using GraphPad ($p$ <0.05 was considered statistically significant).

### 4.3.11 ROS generation assay in 4T1 cells

The ROS generation assay was performed by DCFHDA assay to understand the photodynamic therapy of the developed compound in the presence and absence of NIR laser. In a 96-well cell culture plate, 6,000 cells were plated and incubation was carried out for 24 h at 37 °C. Afterwards, the next day, cells were treated with NDLA-AuNCs and irradiated with 690 nm laser for 10 minutes. The cells were incubated for 3 hours and then were stained with 10 μM DCFHDA and imaged using live cell imager and quantified using ImageJ.

**4.3.12 Mitochondrial damage using JC-1 assay:**

In a 96-well cell culture plate, 6,000 cells were plated and incubation was carried out for 24 h at 37 °C. Afterwards, the next day, cells were treated with NDLA-AuNCs and incubated for 6 hours. Later, the cells were incubated with 10 μg/mL JC-1 stain for 20 mins and the washed again and imaged under a live cell imager and quantified using ImageJ

**4.3.13 *In vivo* Cytotoxicity and Histopathology**

The *in vivo* cytotoxicity and biocompatibility studies of the NDLA-AuNCs have been conducted using male BALB/c mice [n= 6 (three for control and three for treated mice)]; body weight: 25± 5 g). The adult male BALB/c mice were housed in polypropylene cage (Tarson, India) and were brought 30 days before the experiments for acclimatization by providing with normal healthy diet and water *ad libitum*. The study was conducted under the supervision of Institutional Animal Ethics Committee (IAEC) (IRM/2024/IAEC/M8/26/12/2024) complying with the standardized guidelines of the Committee for Control and Supervision of Experiments on Animals (CCSEA), Government of India and International guidelines of Organization for Economic Co-Operation and Development (OECD) for animal care and use. To determine the adversity and systemic toxicity of the NDLA-AuNCs, a prepared suspension (2 $mg \cdot kg^{-1}$) were orally administrated by gavage feeding once daily for fourteen days (cumulative dose: 28 $mg \cdot kg^{-1}$). Post, fourteen days of treatment, mice were euthanized, and blood samples were collected for determining clinical alterations caused by the AuNCs.

The major organs (heart, spleen, kidney, and liver) were collected, and fixed in 4% neutral buffered formalin, embedded in paraffin. Then the organs were sectioned, and stained with hematoxylin and eosin (H&E) for histopathological analysis.

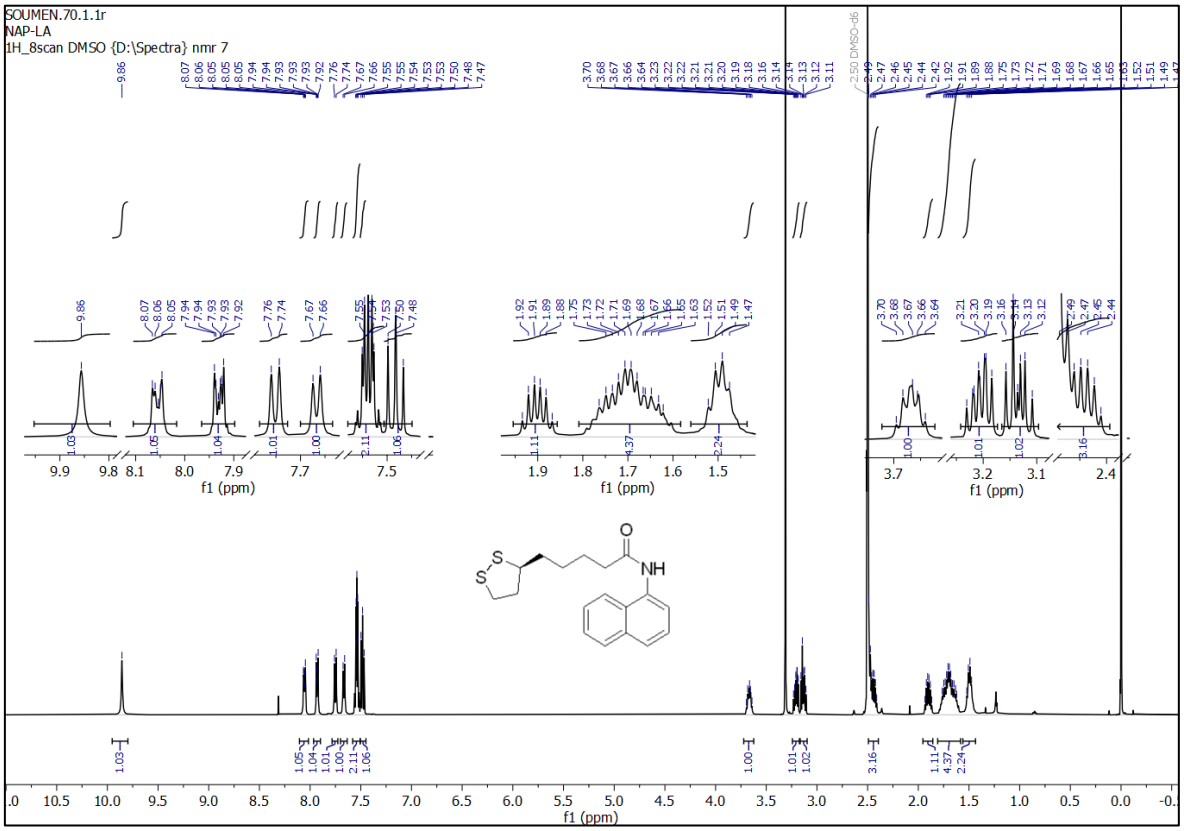


**Figure S1** $^{1}$H NMR of the ligand (NDLA).

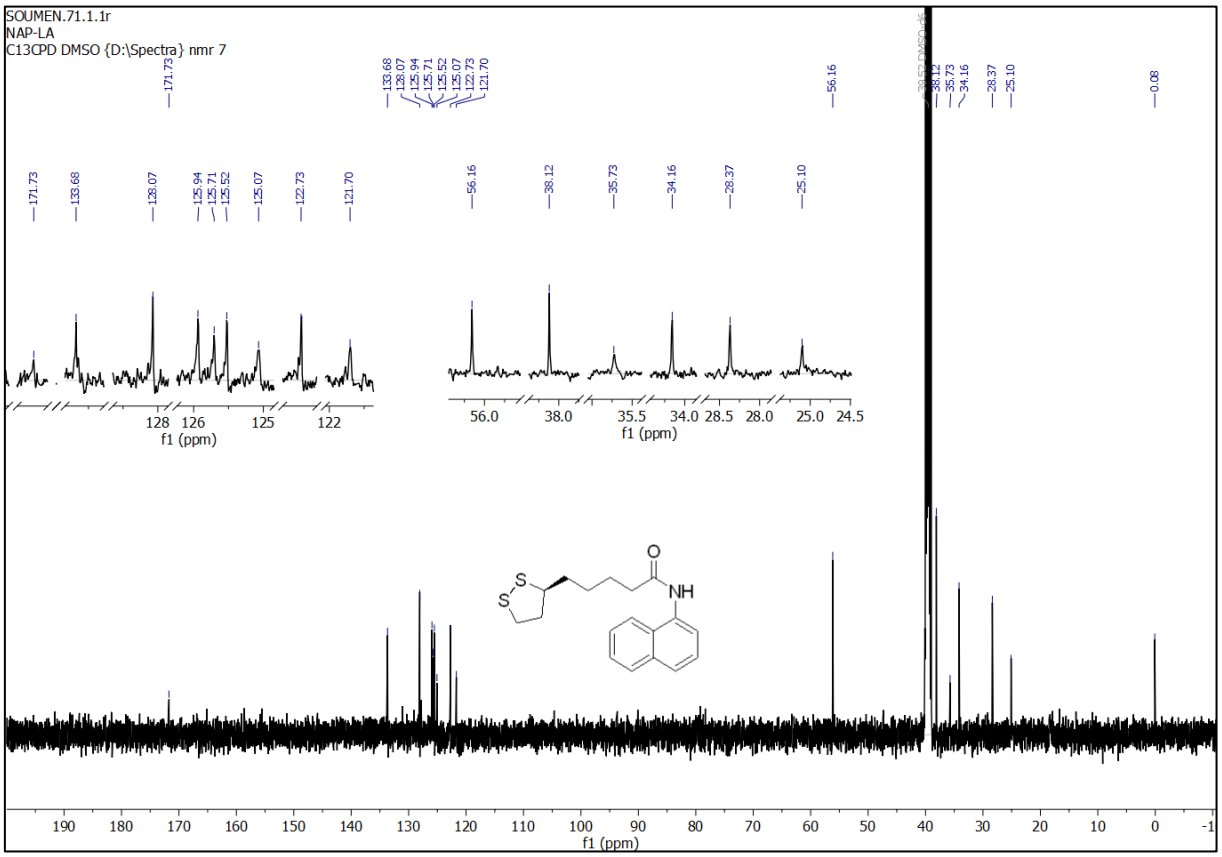


**Figure S2** $^{13}$C NMR of the ligand (NDLA).

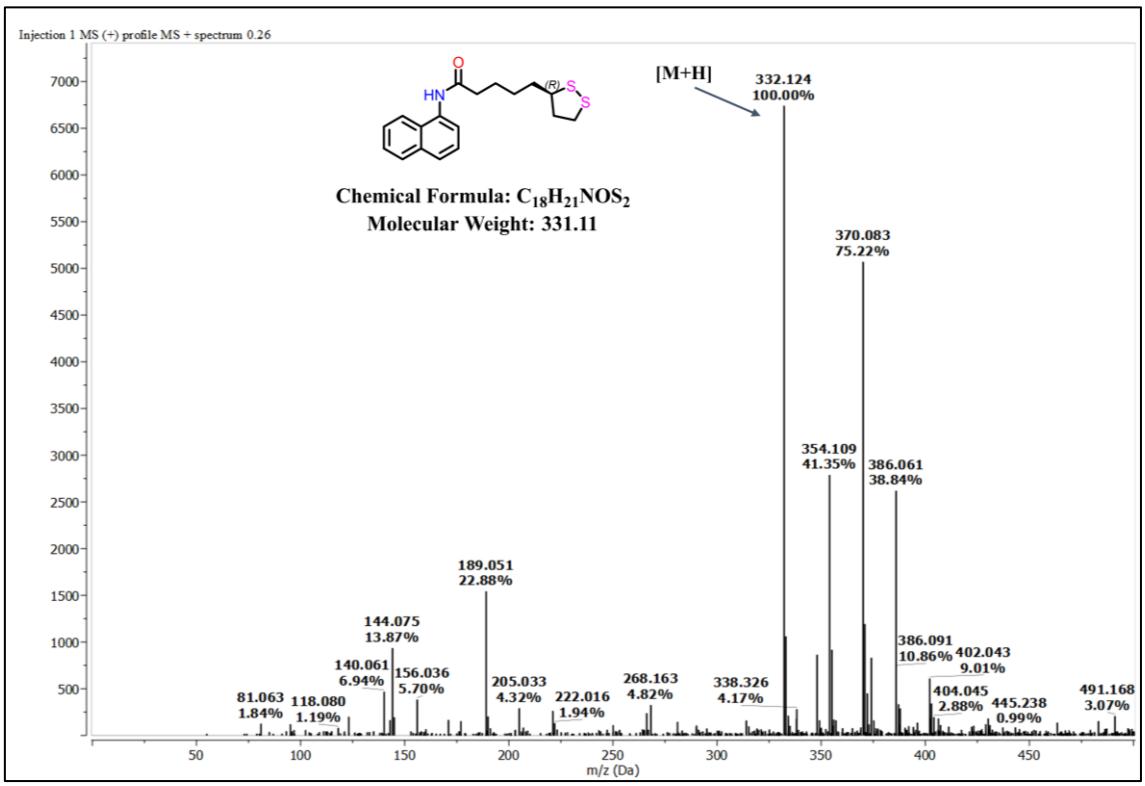


**Figure S3** Mass spectroscopy of the ligand (NDLA).

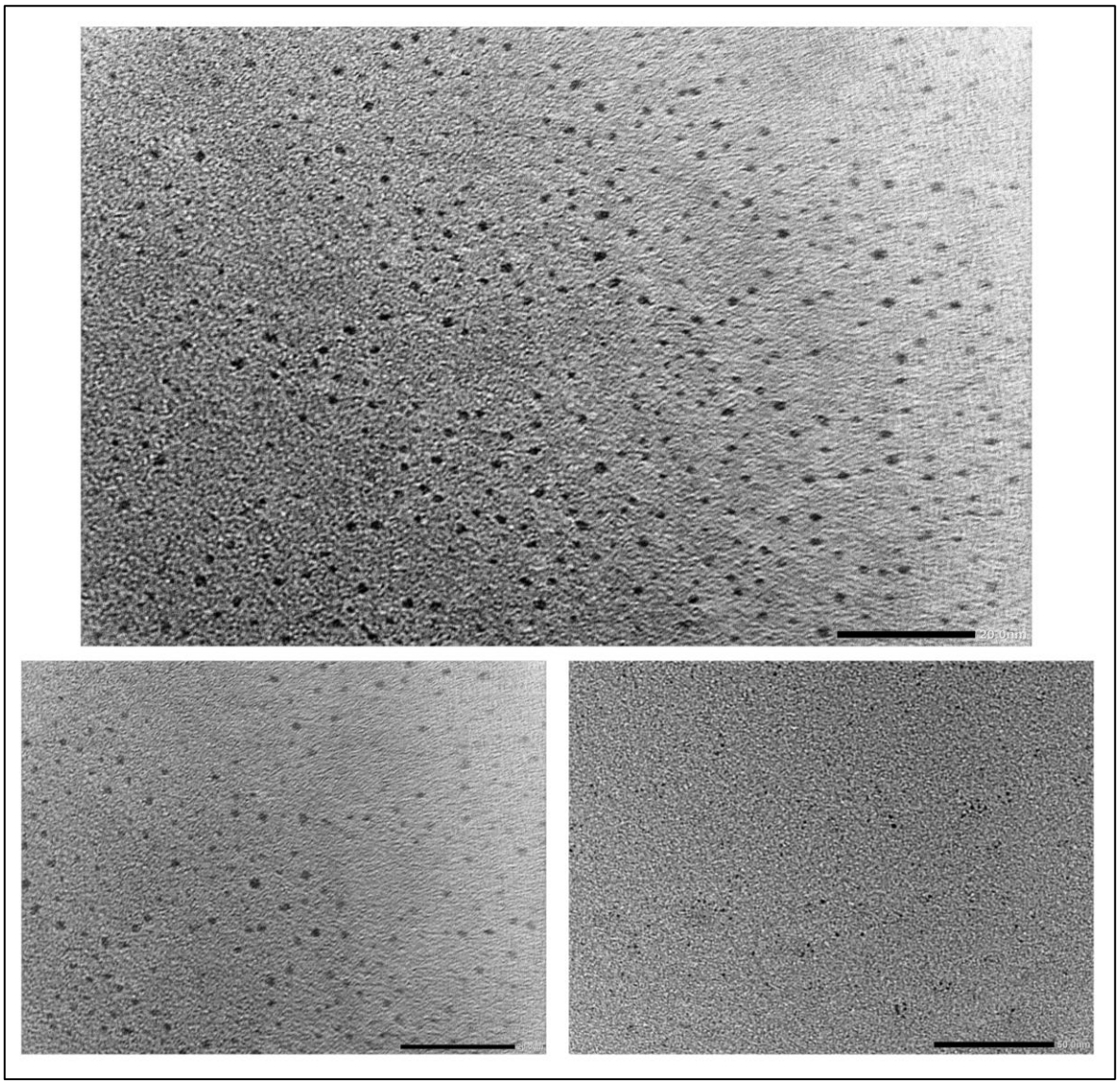

**Figure S4** High-Resolution Transmission Electron Microscopy (HRTEM) image of AuNCs (@ 20 nm & 50 nm Scale).

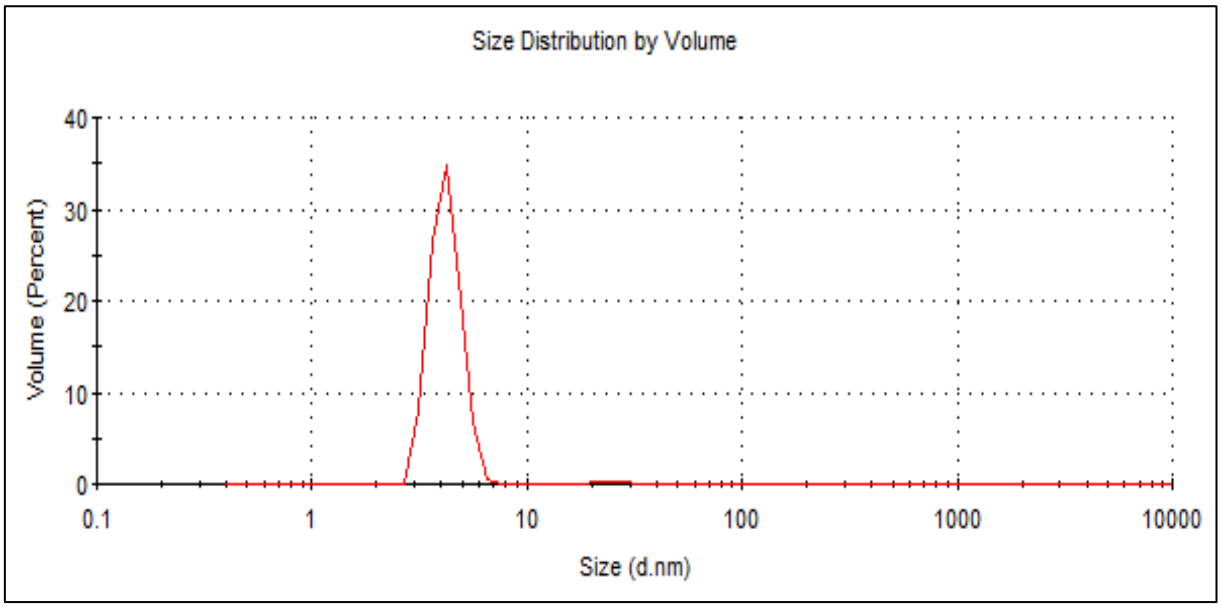


**Figure S5** Dynamic Light Scattering (DLS) study of AuNCs showing hydrodynamic diameter of 4.1 nm.

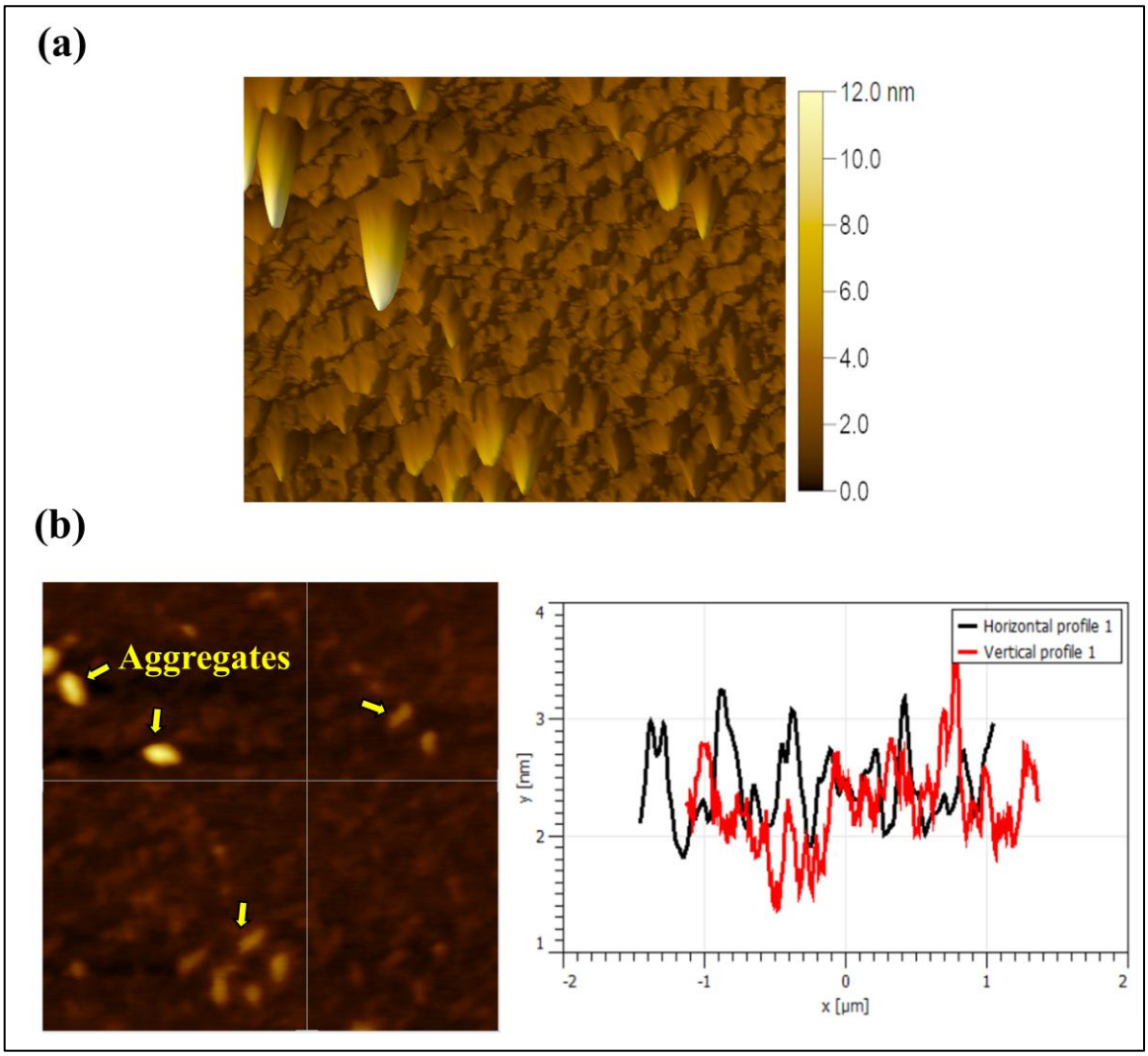


**Figure S6** (a) Surface morphology analysis of AuNCs using AFM, (b) corresponding height distribution graphs (red colour for vertical profile; black colour for horizontal profile) of AuNCs.

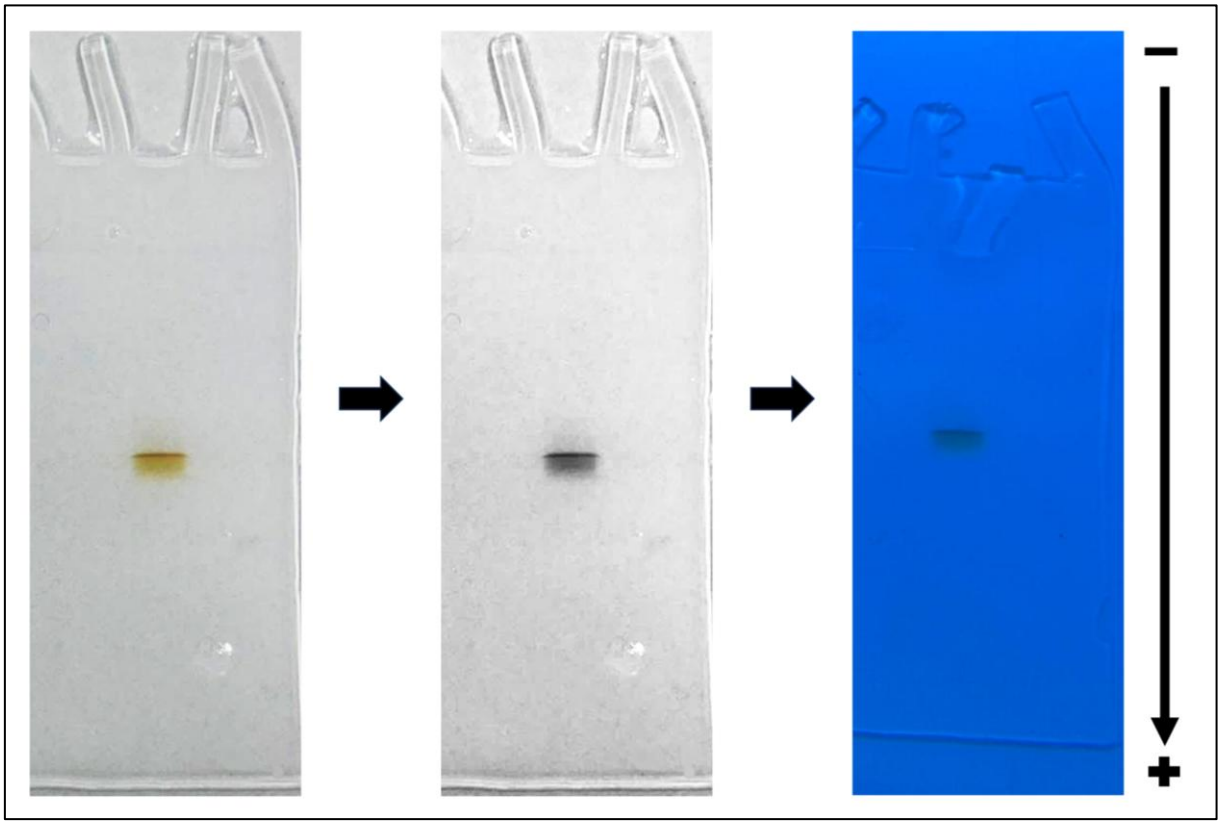

**Figure S7** Native Polyacrylamide Gel Electrophoresis (PAGE) study of AuNCs, showing distinct single band (from left to right, photographs of PAGE under normal light, gel-dock, and UV light).

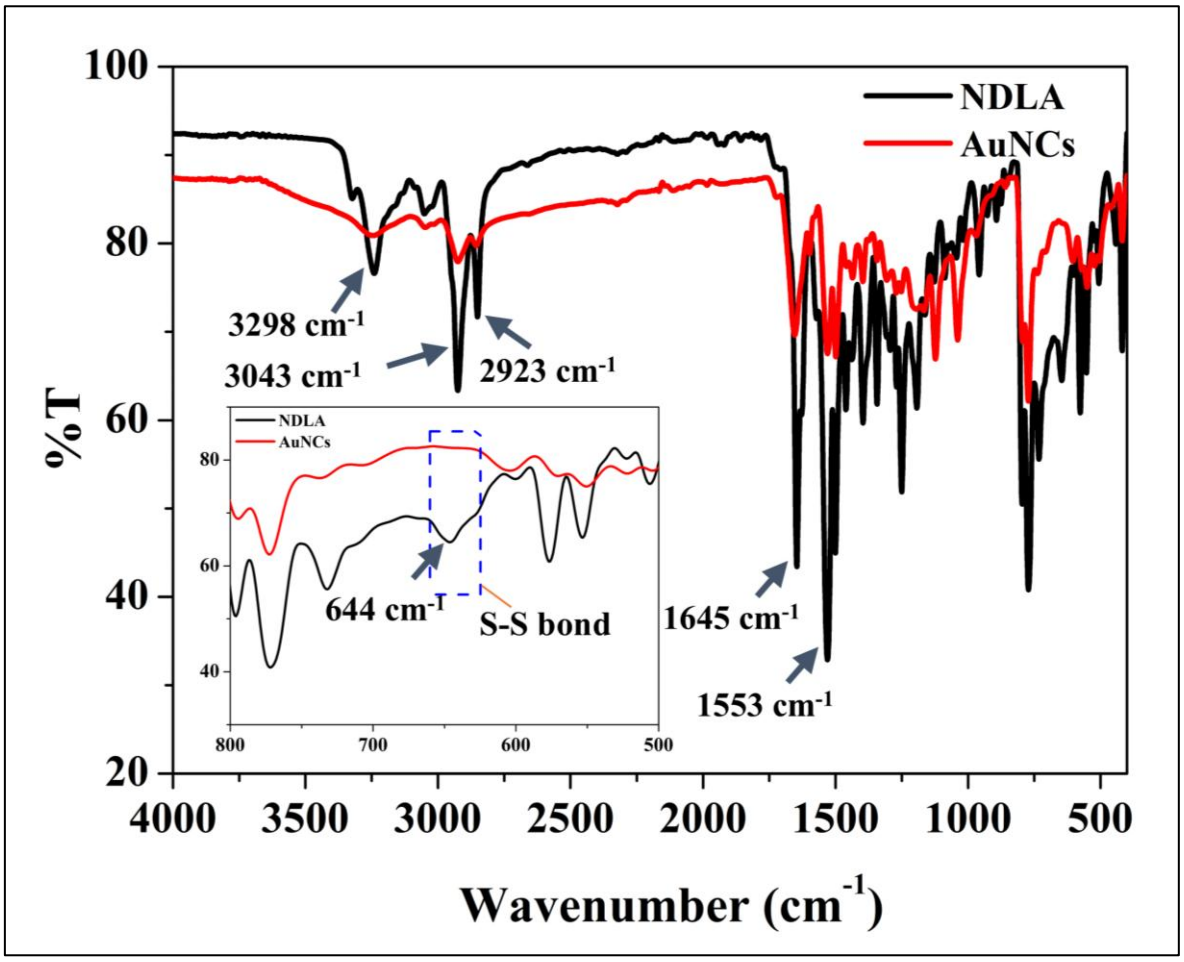


**Figure S8** Fourier transform infrared (FTIR) spectra of NDLA ligand and AuNCs (Inset image displayed the characteristic disulfide band completely disappears upon completion of the AuNCs formation).

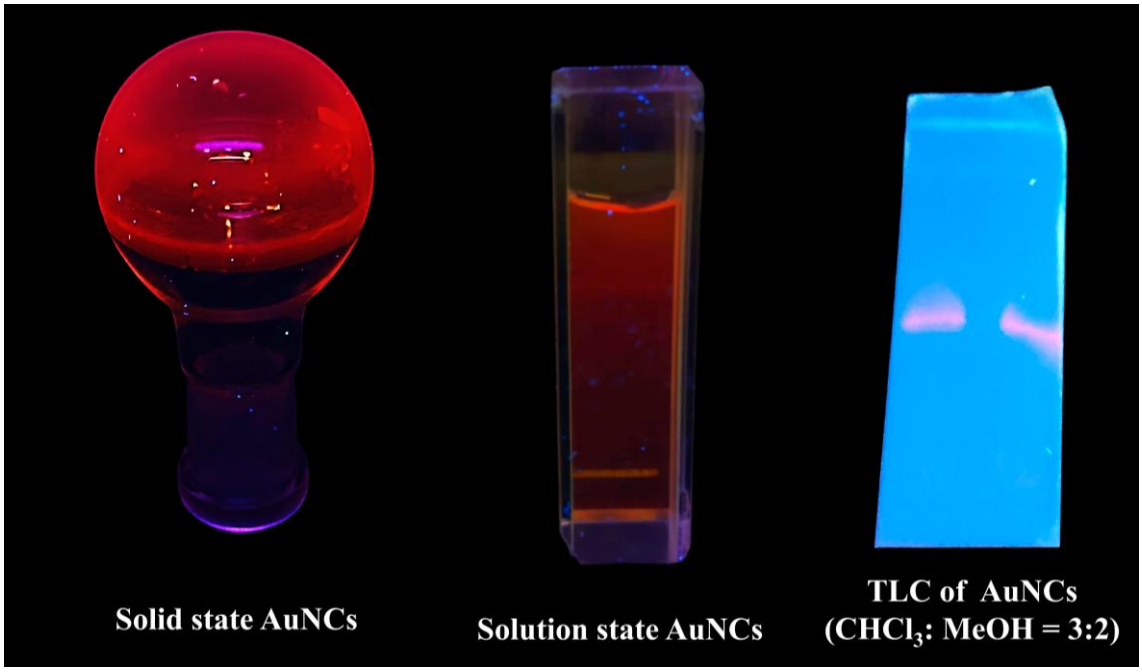


**Figure S9** Images of AuNCs in solid state (left side), solution state (middle)and thin layer chromatography (TLC) using CHCl3: MeOH (3:2) eluent (right side), under 365 nm UV light.

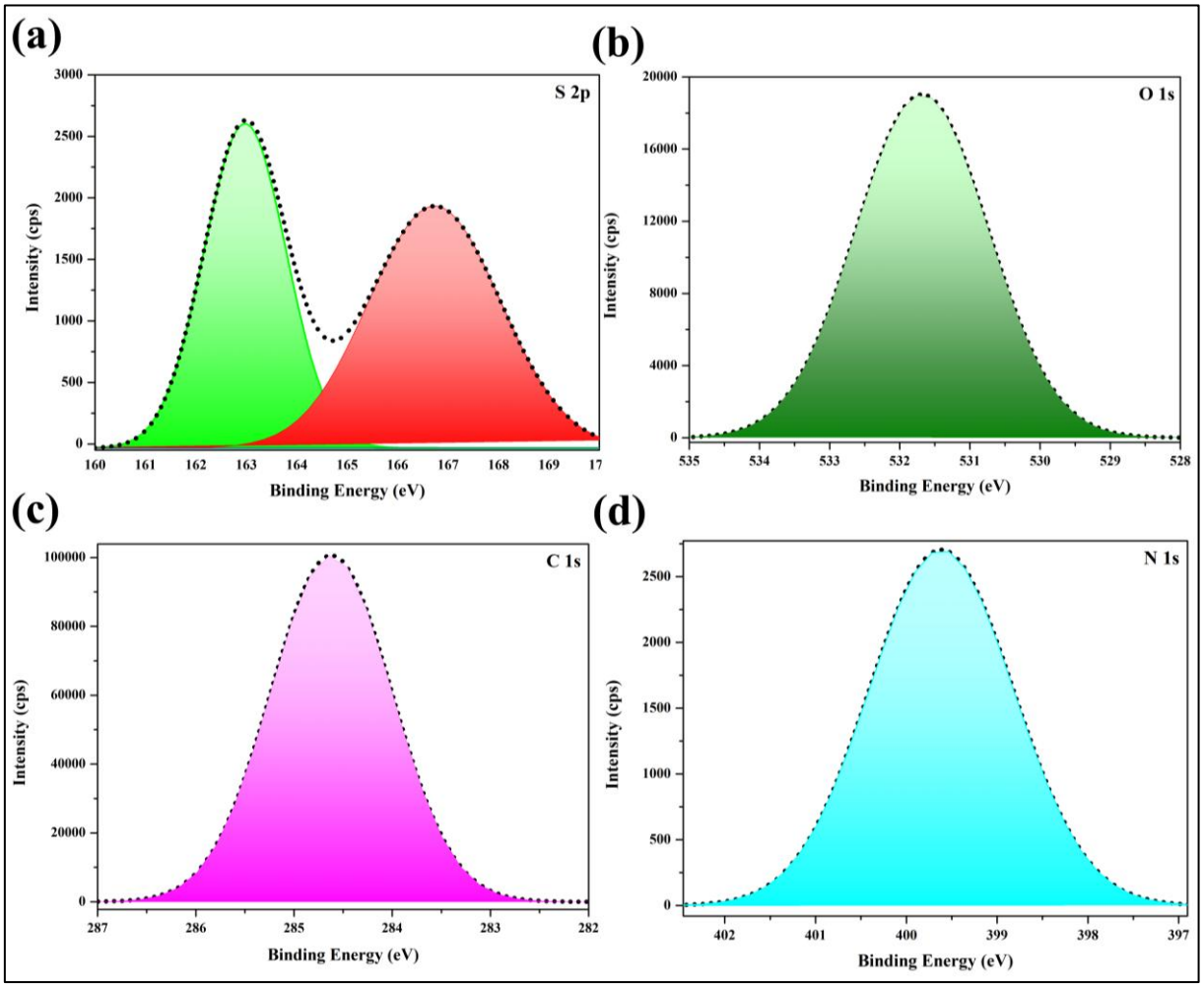


**Figure S10** X-ray photoelectron spectroscopy (XPS) spectra of (a) sulfur, (b) oxygen, (c) carbon, and (d) nitrogen elements in AuNCs.

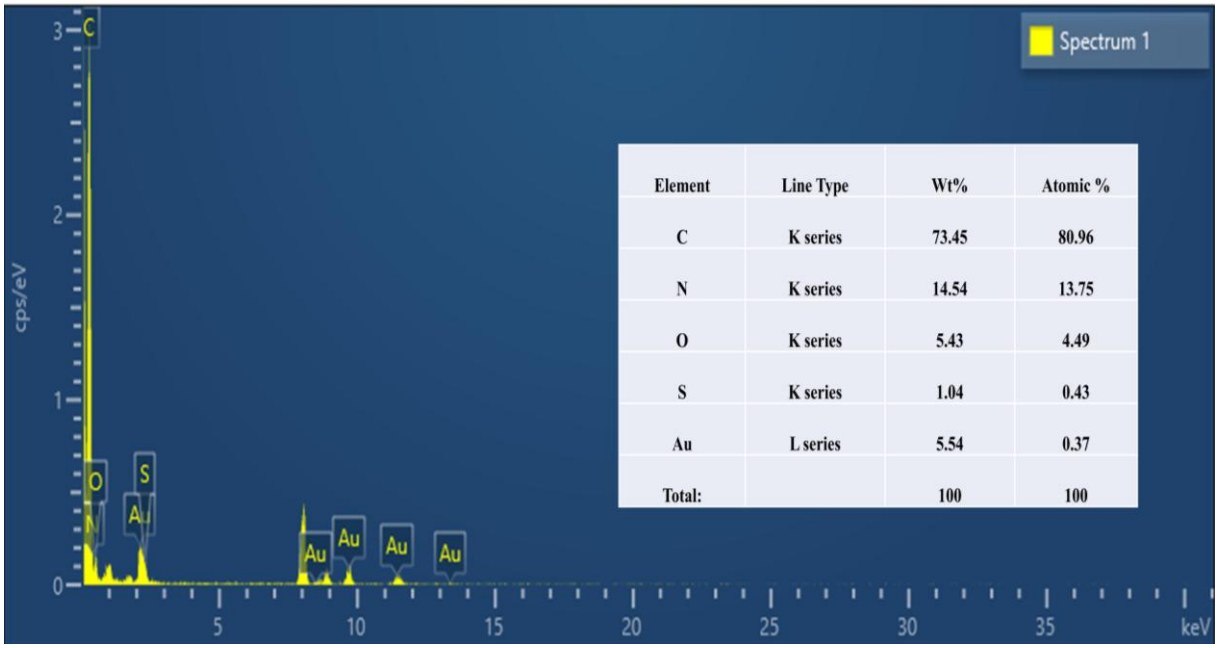


| Element | Line Type | Wt% | Atomic % |
|---|---|---|---|
| C | K series | 73.45 | 80.96 |
| N | K series | 14.54 | 13.75 |
| O | K series | 5.43 | 4.49 |
| S | K series | 1.04 | 0.43 |
| Au | L series | 5.54 | 0.37 |
| Total: | | 100 | 100 |

**Figure S11** Energy-dispersive X-ray spectroscopy (EDS) spectra of AuNCs.

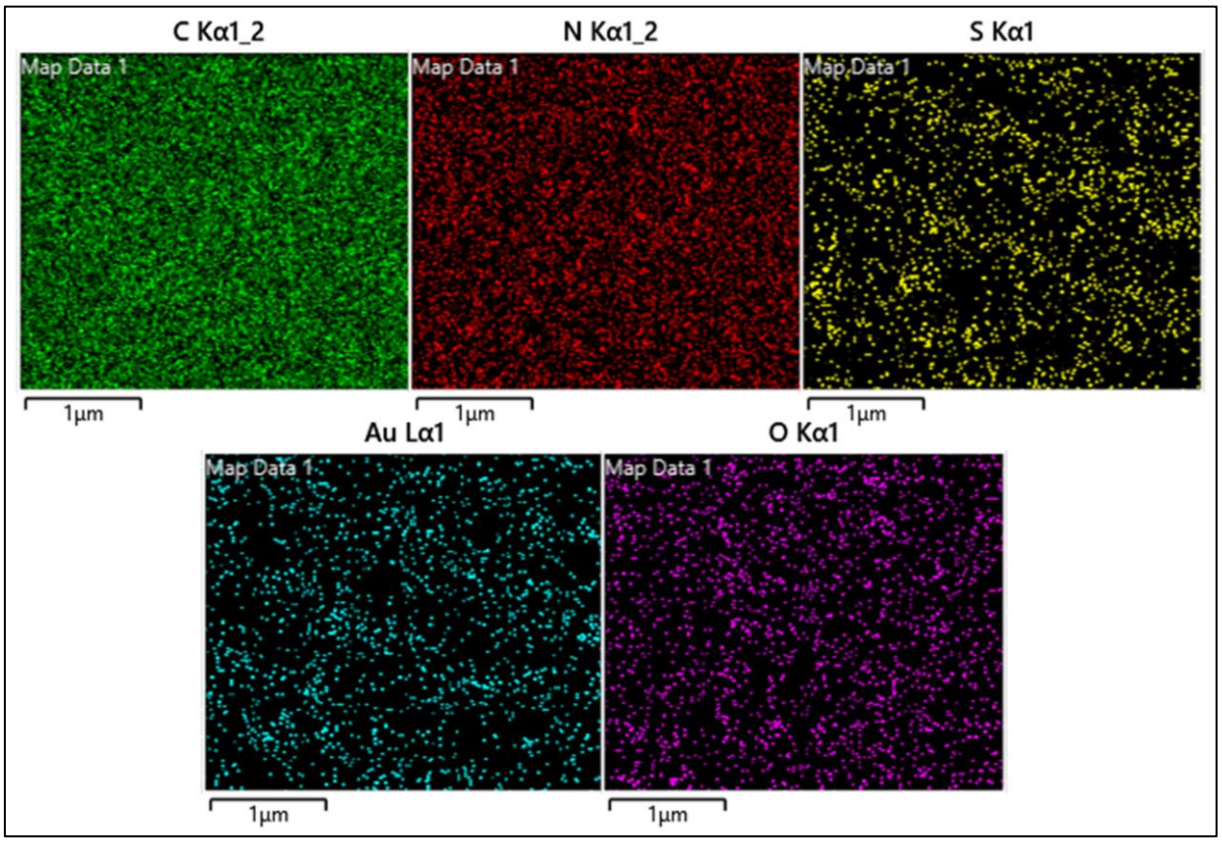


**Figure S12** Elemental mapping of AuNCs showing presence of carbon (C), nitrogen (N), sulfur (S), gold (Au), and oxygen (O) elements.

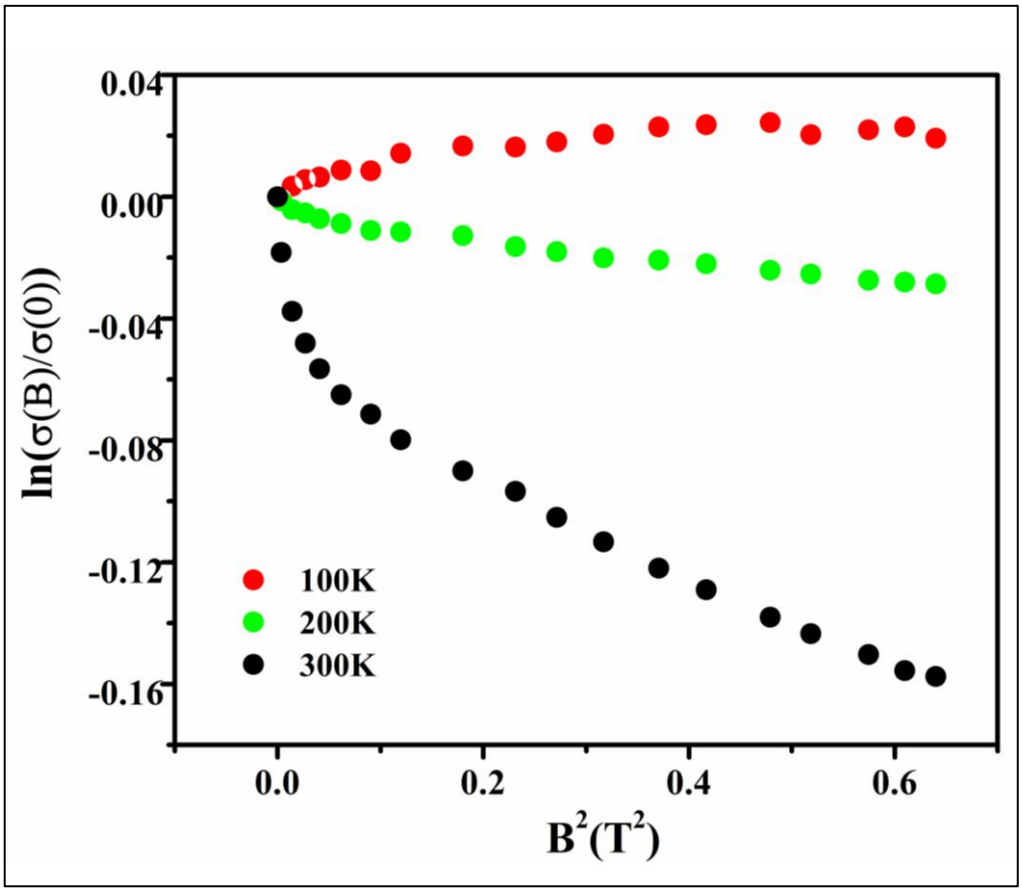


**Figure S13** Wave function shrinkage model showing the electrons are contracted under the influence of magnetic field.

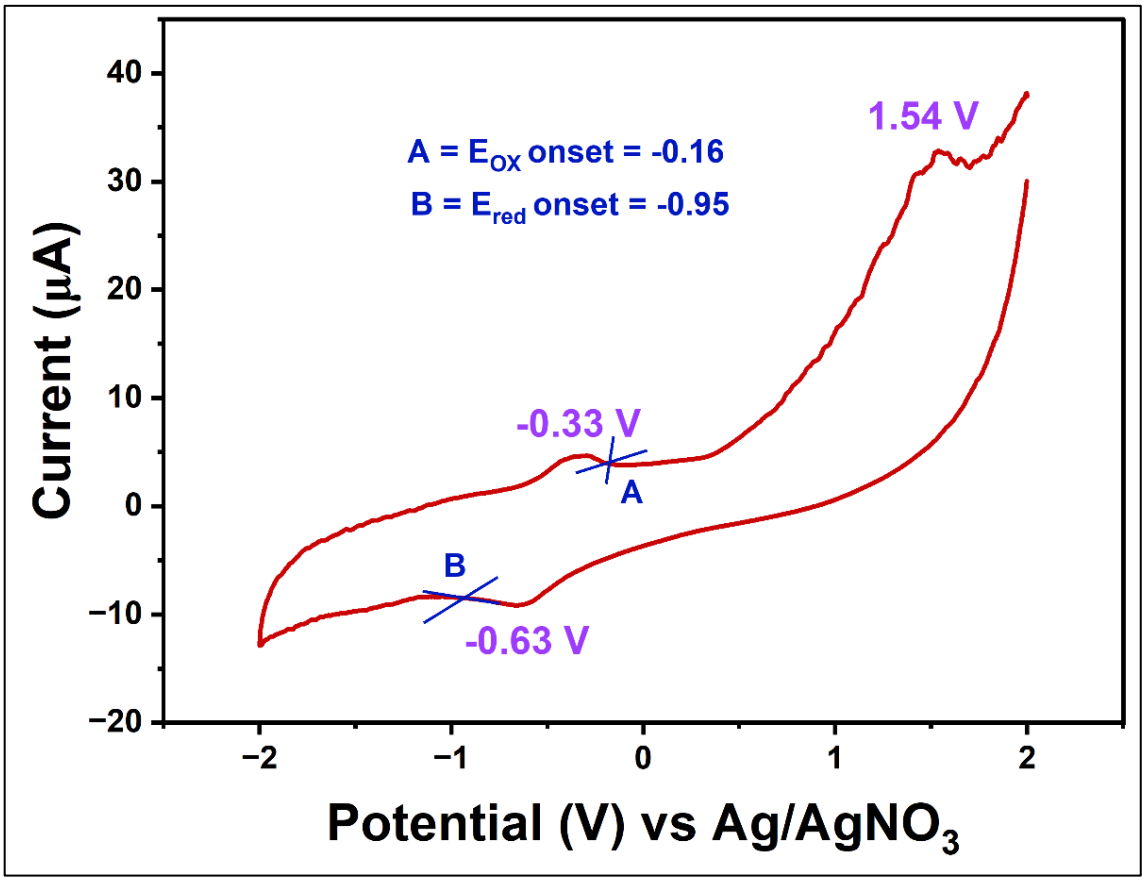


**Figure S14** Cyclic voltammetry for AuNCs in a 0.1 M TBAF electrolyte containing solution of acetonitrile.

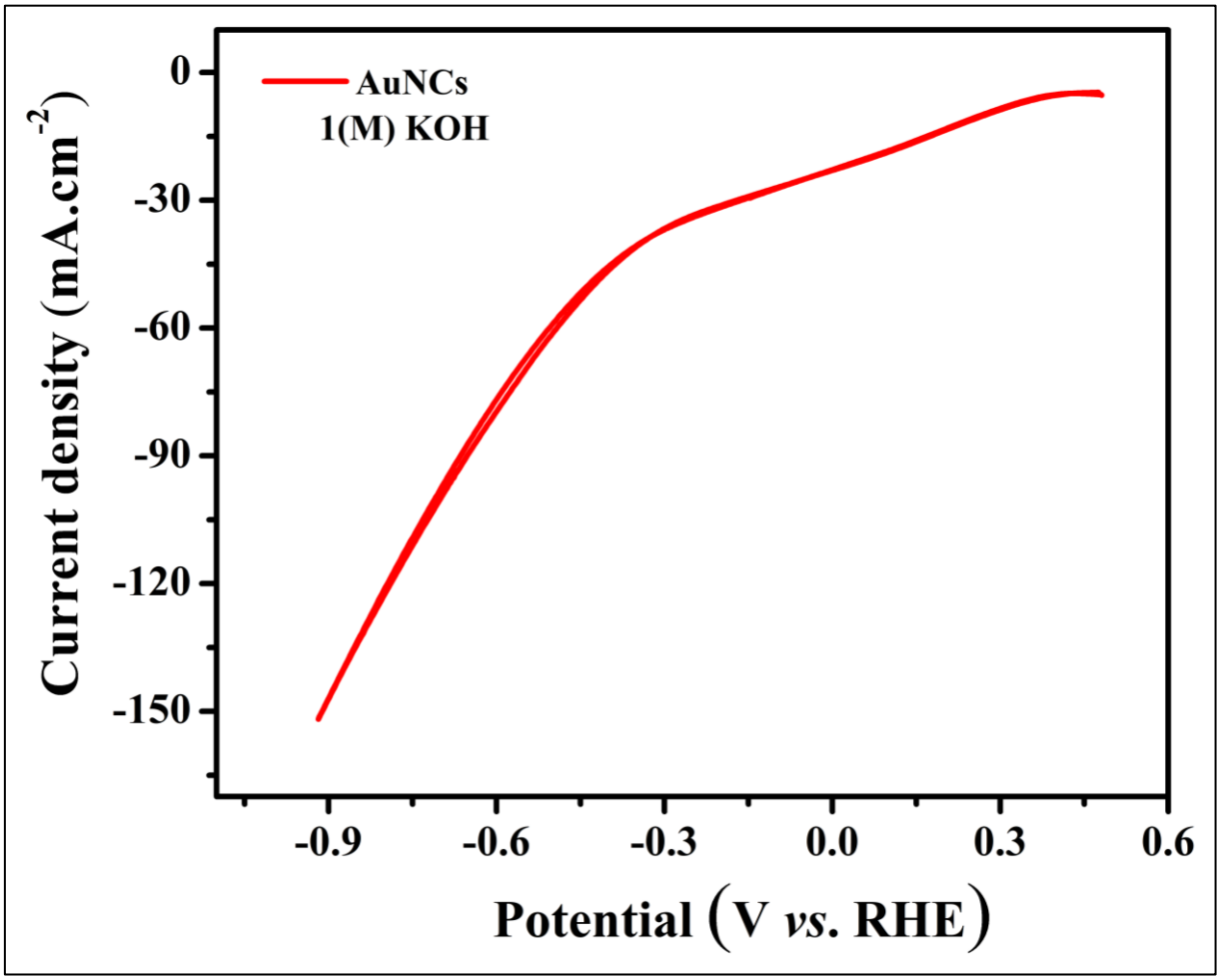


**Figure S15** Cyclic voltammetry (CV) curves for HER analysis in 1 (M) KOH.

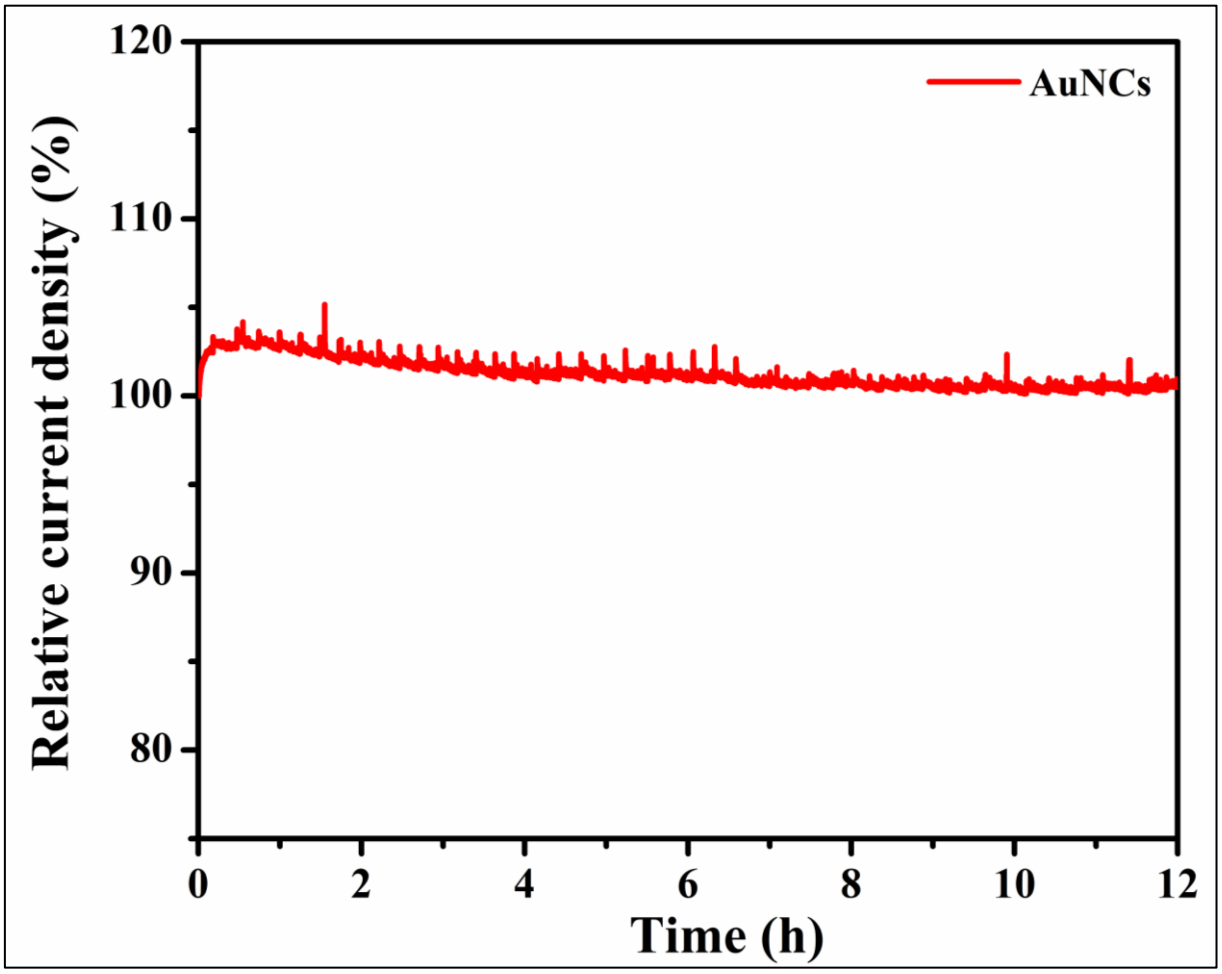


**Figure S16** Relative current density plot showing initial current density largely retained after 12 hours.

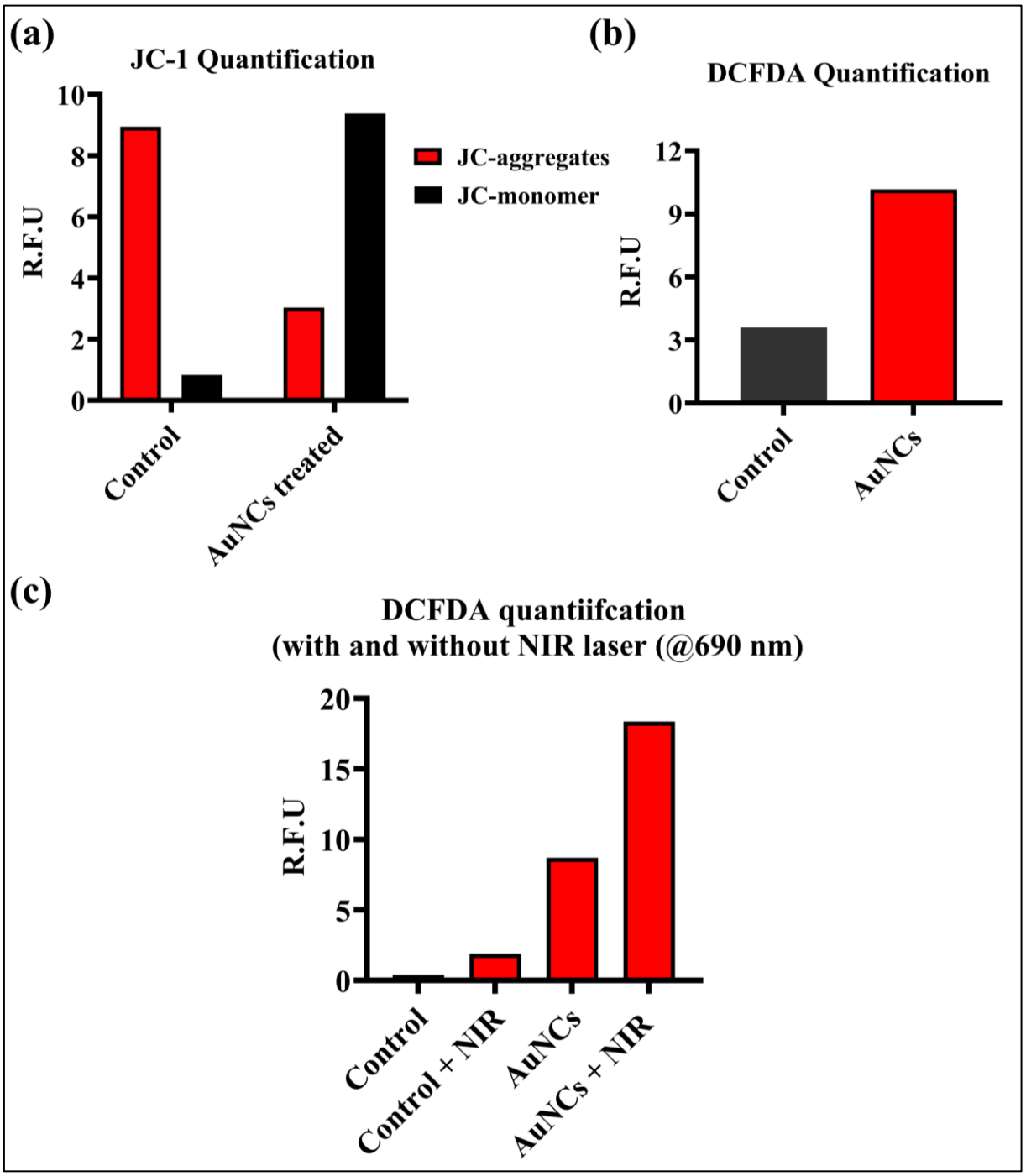


**Figure S17** Spectroscopic quantifications of (a) JC-1 assay including JC-aggregates (red colour), and JC-monomer (green colour). (b) ROS generation using DCFDA assay; (c) photodynamic activity and ROS-quantification at 690 nm NIR laser using DCFDA assay.

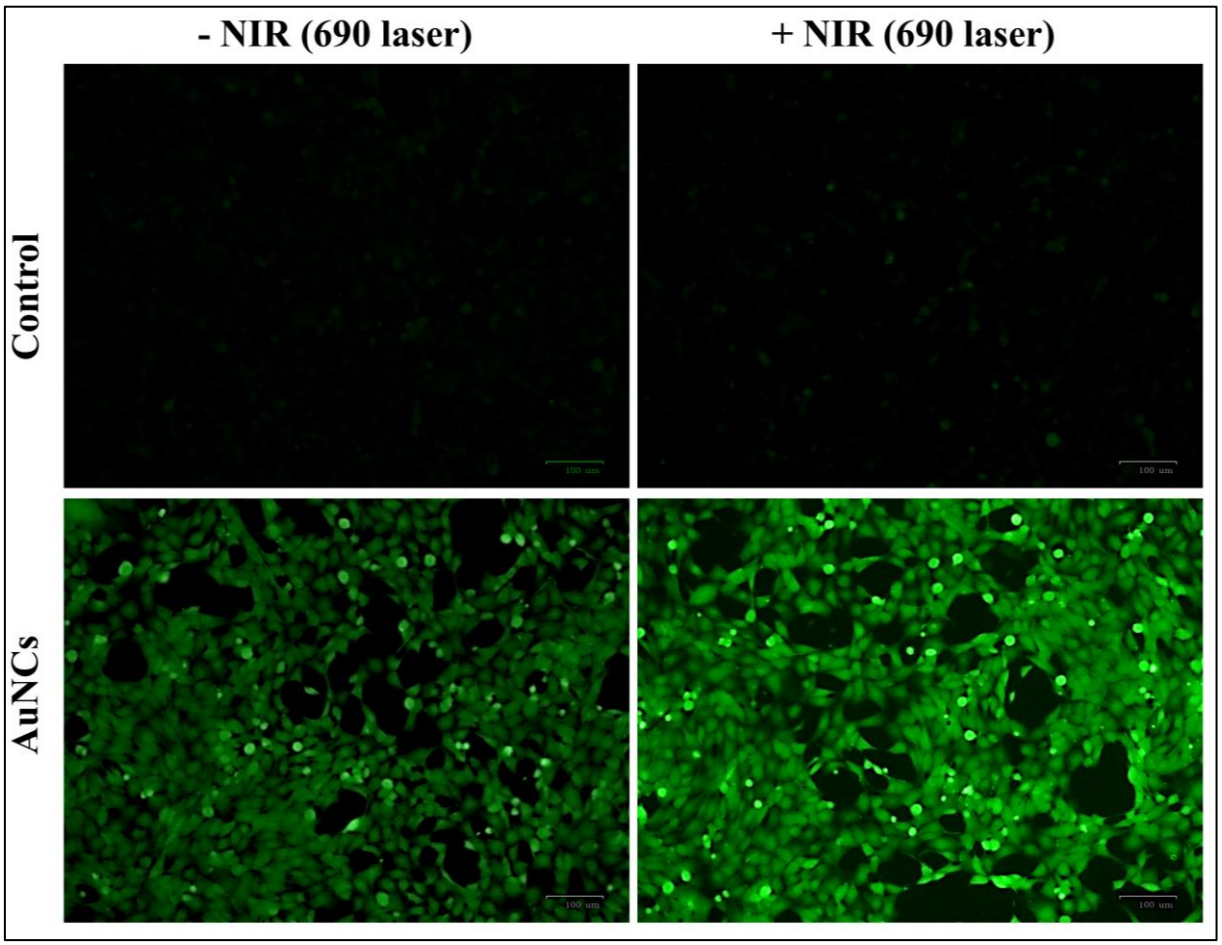


**Figure S18** *In vitro* photodynamic activity analysis of AuNCs using 690 nm laser in 4T1 cell lines treated with DCFDA dye (working conc. 0.1 mg·mL$^{-1}$ AuNCs).

**Table S1** Statistical results of AFM analysis.

| **Parameters** | | **Integrals** | |
|---|---|---|---|
| **Minimum** | 1.82087 nm | **Projected length** | 2.50000 μm |
| **Maximum** | 3.24987 nm | **Developed length** | 2.50009 μm |
| **Mean value** | 2.43381 nm | **Variation** | 16.3656 nm |
| **Median** | 2.38221 nm | **Mean value** | 2.43341 nm |
| **Ra** | 269.713 pm | **Area under curve** | 6083.52 nm² |
| **Rms (Rq)** | 324.194 pm | **Positive area** | 6083.52 nm² |
| **Skew** | 0.437552 | **Negative area** | 0.000000 m² |
| **Excess kurtosis** | 0.538684 | **Root mean square** | 2.45484 nm |

**Table S2** Comparison of overpotential for hydrogen evolution reaction (HER) with reported bare gold nanoclusters (AuNCs).

| No | Gold Nanoclusters (AuNCs) | Ligand family | Size (nm) (TEM) | Overpotential ($\eta_{10}$) | Reference |
|---|---|---|---|---|---|
| **1** | **$Au_{77}(SC_1P)_8$** | Thiolated porphyrin | 1.3 | **470** | 1 |
| **2** | **$Au_{75}(SC_1P)_{11}$** | Thiolated porphyrin | 1.3 | **500** | 1 |
| **3** | **$Au_{25}(SR)_{18}$** | Alkyl thiol | 0.9 | **693** | 2 |
| **4** | **$Au_{38}(SR)_{24}$** | Alkyl thiol | 1.07 | **635** | 2 |
| **5** | **$Au_{25}(C_{12}T)_{18}$** | Alkyl thiol | 0.9 | **710** | 3 |
| **6** | **$Au_{25}(SC_6H_{13})_{18}$** | Alkyl thiol | | **541** | 3 |
| **7** | **$Au_{25}(PET)_{18}$** | Aromatic thiol | 0.9 | **501** | 3 |
| **8** | **$Au_{38}(PET)_{24}$** | Aromatic thiol | 1.07 | **547** | 3 |
| **9** | **$Au_{130}(PET)_{50}$** | Aromatic thiol | 1.5 | **595** | 3 |
| **10** | **$Au_{144}(PET)_{60}$** | Aromatic thiol | 1.6 | **564** | 3 |
| **11** | **$Au_{25}(MPA)_{18}$** | Alkyl thiol | | **445** | 4 |
| **12** | **$Au_{17}(NDLA)_{10}$** | Chiral aromatic dithiolan | 1.17± 0.22 | **381** | This Work |

**References:**

S1. Eguchi, Daichi, Masanori Sakamoto, and Toshiharu Teranishi. "Ligand effect on the catalytic activity of porphyrin-protected gold clusters in the electrochemical hydrogen evolution reaction." *Chemical Science* 9.1 (2018): 261-265.

S2. Choi, Woojun, et al. "Effects of metal-doping on hydrogen evolution reaction catalyzed by MAu24 and M2Au36 nanoclusters (M= Pt, Pd)." *ACS applied materials & interfaces* 10.51 (2018): 44645-44653.

S3. Kumar, Bharat, et al. "Gold nanoclusters as electrocatalysts: size, ligands, heteroatom doping, and charge dependences." *Nanoscale* 12.18 (2020): 9969-9979.

S4. Luo, Lipan, et al. "Ligand-induced changes in the electrocatalytic activity of atomically precise Au 25 nanoclusters." *Chemical Science* 16.8 (2025): 3598-3610.